Time-delimited signaling of MET receptor tyrosine kinase regulates cortical circuit development and critical period plasticity

Ke Chen[1,3,#], **Xiaokuang Ma**[1,2,#], **Antoine Nehme**[1], **Jing Wei**[1], **Yan Cui**[3], **Yuehua Cui**[1], **Dezhong Yao**[3], **Jie Wu**[1,2,4], **Trent Anderson**[1], **Deveroux Ferguson**[1], **Pat Levitt**[5,*], **Shenfeng Qiu**[1,*]

[1]Basic Medical Sciences, University of Arizona College of Medicine-Phoenix, Phoenix, Arizona, 85004.

[2]Department of Pharmacology, Shantou University Medical College, Shantou, Guangdong, 515041, China.

[3]MOE Key Laboratory for Neuroinformation, The Clinical Hospital of Chengdu Brain Sciences Institute, University of Electronic Science and Technology of China, Chengdu, Sichuan, 610054, China.

[4]Barrow Neurological Institute, St. Joseph's Hospital Medical Center, Phoenix, Arizona, 85013.

[5]Department of Pediatrics and Program in Developmental Neuroscience and Neurogenetics, The Saban Research Institute, Children's Hospital Los Angeles, Keck School of Medicine, University of Southern California, Los Angeles, CA, 90027.

Abstract

Normal development of cortical circuits, including experience-dependent cortical maturation and plasticity, requires precise temporal regulation of gene expression and molecular signaling. Such regulation, and the concomitant impact on plasticity and critical periods, is hypothesized to be disrupted in neurodevelopmental disorders. A protein that may serve such a function is the MET receptor tyrosine kinase, which is tightly regulated developmentally in rodents and primates, and exhibits reduced cortical expression in autism spectrum disorder and Rett Syndrome. We found that the peak of MET expression in developing mouse cortex coincides with the heightened period of synaptogenesis, but is precipitously down-regulated prior to extensive synapse pruning and certain peak periods of cortical plasticity. These results reflect a potential on-off regulatory

*Corresponding authors: Pat Levitt plevitt@med.usc.edu, Shenfeng Qiu sqiu@email.arizona.edu.
#These authors contributed equally to this work.

synaptic mechanism for specific glutamatergic cortical circuits in which MET is enriched. In order to address the functional significance of the 'off' component of the proposed mechanism, we created a controllable transgenic mouse line that sustains cortical MET signaling. Continued MET expression in cortical excitatory neurons disrupted synaptic protein profiles, altered neuronal morphology, and impaired visual cortex circuit maturation and connectivity. Remarkably, sustained MET signaling eliminates monocular deprivation-induced ocular dominance plasticity during the normal cortical critical period; while ablating MET signaling leads to early closure of critical period plasticity. The results demonstrate a novel mechanism in which temporal regulation of a pleiotropic signaling protein underlies cortical circuit maturation and timing of cortical critical period, features that may be disrupted in neurodevelopmental disorders.

Keywords

INTRODUCTION

Dysregulated synapse development and cortical circuit function is a hallmark pathology of many neurodevelopmental and neuropsychiatric disorders, including autism spectrum disorders (ASD) (1, 2). The human *MET* gene, which encodes a receptor tyrosine kinase, MET, has emerged as a neurodevelopmental component that influences circuit function in rodents and primates. The human rs1858830 'C' allele in *MET* promoter reduces gene transcription by 50% (3). Consistently, MET protein levels are reduced by approximately 50% in postmortem temporal cortical tissue from individuals with ASD (4, 5) and nearly absent in individuals with Rett Syndrome (6). Human neuroimaging also demonstrates that the *'C'* allele modulates both functional and structural cortical connectivity in typically developing individuals and people with ASD, with a greater impact on the latter individuals (7).

These observations have led to investigations determining the developmental mechanisms through which MET confers phenotypic risk. In primates and mice, MET is expressed in subpopulations of cortical neurons for limited periods of time during development, peaking during synaptogenesis and exhibiting dramatic reductions during synapse stabilization and pruning (8, 9). This occurs in specific circuits, as MET expression is enriched in intratelencephalic cortico-cortical neurons (in layers 2–3 and 6), and corticostriatal neurons (in layer 5) (10). The early period of high expression coincides with heightened neuronal structural changes including rapid neurite growth, synapse formation and elimination (11). The potential role of MET in mediating synapse maturation and plasticity has been investigated in the developing mouse hippocampus (12), in which expression is temporally regulated. Enhanced or reduced MET signaling in single developing hippocampal CA1 neurons leads to opposing changes of dendritic spine size and density, and time course of maturation (13).

In all species examined thus far, the neurobiological timeframe of MET expression in the neocortex is highly conserved. One outstanding question is whether the time-delimited

signaling, particular its transient nature, is functionally critical for circuit development. We hypothesized that timely termination of MET signaling is a highly regulated event that facilitates further cortical circuit development. Towards addressing this hypothesis, we created a controllable transgenic mouse line, in which the *Met* transgene can be turned on to extend signaling duration after the endogenous *Met* gene is switched off. Here, investigation of this model, combined with experiments in the cortical *Met* conditional knockout mice (cKO), reveals that extension or elimination of *Met* signaling results in robust and distinct alterations in synaptic molecular constituents, neuronal morphology, intracortical circuit maturation and connectivity, and perhaps most remarkable, the timing of visual cortex critical period plasticity. These findings have implications for understanding developmental and phenotypic heterogeneity, in which disturbing a single pleiotropic disease risk gene may be responsible for diverse phenotypic outcomes.

MATERIALS AND METHODS

Animals

C57Bl/6J mice were purchased from The Jackson Laboratories. The forebrain-specific conditional mutant mice (cKO, $Met^{fx/fx}$; $emx1^{cre}$) were generated as noted previously (8, 13), by breeding homozygous female $Met^{fx/fx}$ mice to hemizygote $Met^{fx/+}$ male mice with an $emx1^{Cre}$ knock-in allele (14). An approximately equal number of male and female mice were used in this study. Generation of the controllable transgenic mouse line for sustained/ over-expression of *Met* is described in Supplemental materials. To determine number of mice used, power analysis was conducted using an R script that takes pre-specified effect size, expected variations, and type I and II errors as input arguments. Mice of desired genotypes are assigned to experimental groups randomly using a random number generator in MATLAB. Where applicable, mice IDs and data are coded during experiments and analyses so that the experimenters are blinded to genotypes and grouping. All experimental procedures using mice conforms to NIH guidelines and are approved by the Institutional Animal Care and Use Committee of the University of Arizona.

Western blot and biochemical analyses

A standard Western blot protocol was employed to quantify protein levels with specific antibodies (15). For pups less than P14, we dissected out the tissue from desired forebrain regions. For mice older than P14, coronal brain slices (350μm thickness) were first made, followed by collection of region-specific tissue punches. Tissues were sonicated in cell lysis buffer containing proteinase inhibitor cocktail (1:50, Sigma P8340). Protein concentration was assessed using a micro-BCA (ThermoFisher) assay. 10μg tissue samples were separated on 4–15% SDS-polyacrylamide gels, incubated with specific primary and secondary antibodies (Supplemental Materials). Signals were developed using an enhanced chemiluminescence method, captured by ECL Hyperfilm, and quantified using ImageJ.

Whole cell patch clamp recording

Coronal slices containing the visual cortex were used for recording, as described previously (16, 17) (Supplemental Materials). Slices were made in ice-cold ACSF (saturated with 95% O2 and 5% CO2; containing in mM, 126 NaCl, 2.5 KCl, 26 $NaHCO_3$, 2 $CaCl_2$, 1 $MgCl_2$,

1.25 NaH$_2$PO$_4$, and 10 glucose), visualized under a 4X objective to allow anatomical identification of the binocular region of the primary visual cortex (bV1). L5 neurons at least 50 μm below the slice surface were selected for whole cell recordings under a 60X objective (NA = 0.9). Neuronal responses were collected using a MultiClamp 700B amplifier, low-pass filtered at 1kHz (current signals) or 10kHz (voltage signals) and digitized at 20 kHz using a Digidata 1440A interface (Molecular Devices). To record excitatory postsynaptic currents (mEPSCs), slices were perfused with D-AP5 (50μM) and tetrodotoxin (TTX, 1μM, Tocris-Cookson). The electrode internal solution contained (in mM): 130 K-gluconate, 4 KCl, 2 NaCl, 10 HEPES, 4 ATP-Mg, 0.3 GTP-Na, 1 EGTA and 14 phosphocreatine (pH 7.2, 295 mOsm). To measure inhibitory postsynaptic currents (mIPSCs), CNQX (10μM) and TTX were added to the perfusate, and the electrode internal solution contained (in mM): 125 KCl, 2.8 NaCl, 2 MgCl$_2$, 2 Mg^{2+}-ATP, 0.3 Na$_3$GTP, 10 HEPES, 1 EGTA and 10 phosphocreatine (pH 7.25, ~300 mOsm). To obtain stimulus-evoked synaptic responses, a bipolar stimulating electrode (FHC) was placed in layer 2/3 of the bV1, and evoked monosynaptic responses were obtained while L5 pyramidal neurons were voltage clamped at −70 mV (AMPAR-mediated synaptic currents) or + 40 mV (AMPAR+NMDAR) with a Cs+-based internal solution (contains in mM, 125 Cs-gluconate, 5 TEA-Cl, 10 HEPES, 2.5 CsCl, 8 NaCl, 5 QX314-HCl, 4 Mg^{2+}-ATP, 0.3 Na$_3$GTP, 1 EGTA and 10 phosphocreatine, pH 7.25). The morphology of recorded neuron was revealed by including 0.25% biocytin in the electrode internal solution, followed by avidin-A488, and Neurolucida and Imaris reconstruction of dendritic arbors and spines, respectively (Supplemental Materials).

Laser scanning photostimulation (LSPS) for cortical circuit mapping

Mice were sacrificed at P25–32, during the VC critical period (18). Slices were perfused in modified ACSF (4 mM Ca^{2+}, 4 mM Mg^{2+}), with 0.2 mM MNI-caged glutamate and 5μM R-CPP at RT. Pyramidal shaped L2/3 neurons were identified under DIC optics and were selected for whole cell recording. LSPS mapping combined with glutamate uncaging were performed with a 4× objective lens (NA 0.16; Olympus) and 20 mW, 1-ms UV laser (355 nm; DPSS Lasers) pulses. Digital images were registered using a CCD camera (Retiga 2000DC, QImaging) unto which a 16 × 16 stimulation grids with 75-μm spacing were overlaid. Electrophysiological signals were amplified with a Multiclamp 700B amplifier and acquired using BNC-6259 data acquisition boards (National Instruments, Austin, TX). Signals were digitized and acquired at 10 kHz. Data acquisition and analysis were controlled by Ephus software, and a collection of MATLAB scripts (19).

Visual cortex critical period plasticity

Single-unit recording combined with monocular deprivation were used to probe developmental cortical plasticity, according to our previous reports (16, 20). Mice from P22-P48 were used at the start of monocular deprivation (MD). Briefly, mice underwent MD surgery by suturing shut the *right* eyelid for 4–5 days at designated ages. The eyelid was then re-opened, and single unit recording in the anatomically defined bV1 (18) was made immediately after eye re-open. Recordings were performed with Epoxylite-coated tungsten microelectrodes (FHC) with tip resistance of 5–10 MΩ, an amplifier (model 1600; A-M Systems), and digitizer (Micro 1401; Cambridge Electronic Design) under light isoflurane (0.5%) anesthesia. The visual stimulus was generated on an LED monitor using custom

MATLAB scripts, and the Psychtoolbox 3.0 package. Responses were evoked with 0.1 cycle per degree (cpd), 95% contrast sinusoidal drifting gratings presented at twelve equal-spaced orientations. Spike responses were sorted offline with Spike2 software (Cambridge Electronics Design, UK). The orientation with the highest spiking frequency was considered the preferred orientation and was used for analysis. Recorded units were classified into OD categories according to the seven-category scheme of Hubel and Wiesel (18, 21). The number of units in each category was summed for each mouse, and the CBI was calculated according to the following formula: CBI = [(n1 − n7) + (2/3)(n2 − n6) + (1/3)(n3 − n5) + N]/2N, where N is the total number of units and nx is the number of units with OD scores of x (18). Group comparisons for CBI were performed using the non-parametric Mann-Whitney's test.

Statistical analysis

Quantitative results were expressed as mean ± s.e.m. (standard error of the mean). Data were processed using Image J, Adobe Creative Cloud, Microsoft Excel, MATLAB and GraphPad Prism 8.0. To test normality and equal variance, Shapiro–Wilk test and F test were used. Student t test or one-way/two-way analysis of variations (ANOVA) was used when data passed normality and equal variance tests. Potential data outliers were identified as those that differ at least three standard deviations from the mean and excluded from analysis. For dendritic arborization/Sholl analysis, a two-way ANOVA was used to assess group effects. Pearson's $\chi 2$ test was used to compare the categorical dendritic spine data. For non-normally distributed data, non-parametric Mann–Whitney U tests were performed to compare two groups. The Kolmogorov-Smirnov (K-S) test was used to compare cumulative distribution of mEPSC amplitudes. $p < 0.05$ was considered statistically significant for all tests.

RESULTS

Precise temporal regulation of MET protein expression across multiple cortical domains

In the mouse neocortex, MET expression is highest during the first two weeks, followed by a sharp down-regulation of expression and abated signaling prior to weaning (8, 22). To address whether there are brain region-specific differences in the timing of MET expression developmentally, Western blot was performed at multiple time points from postnatal day (P) 0 to P42 in the visual cortex (VC) (Fig. 1a). Quantitative analysis reveals that MET expression is highest during the first two weeks in VC, followed by a rapid down regulation by three weeks. MET expression in the prefrontal cortex (PFC) and hippocampus (HPC) follows a similar temporal pattern (Suppl. Fig. 1a); except that both peak expression and down-regulation occurred earlier postnatally in the HPC CA1. These data are consistent with immunohistochemistry staining (Suppl. Fig. 1b – PFC). In acutely prepared PFC brain slices from P7–9 mice, application of hepatocyte growth factor (HGF), the only known ligand for MET receptor tyrosine kinase activation (23), induces rapid activation of MET, as revealed by an increase in phosphorylated MET (pY1234/1235) (24) (Suppl. Fig. 1c). Lastly, in cultured primary neurons prepared from embryonic mice hippocampus (E17), a similar temporal pattern of MET expression is preserved (Suppl. Fig. 1d). These data suggest temporally-regulated MET expression is a conserved, cell-autonomous, and intrinsic

mechanism across cerebral cortical regions, consistent with a functionally significant role in cortical circuit development.

Creation and validation of a controllable *Met* transgenic mouse line

To determine the functional significance of time-delimited MET expression, we designed experiments to address the consequences of extending the normal time period of expression genetically (Fig. 1b). A controllable *Met* transgenic mouse line was engineered (*Met*$^{ctg+}$, see Suppl. Materials), which, when crossed to a CaMKII-tTA line (25), is expected to express MET in cortical excitatory neurons (25, 26). In the transgene construct, *Met* cDNA (NM_00851) was cloned in frame with a Myc-FLAG tag, and its expression was driven by the tetracycline response element (TRE) promoter. By design, transgene expression should be temporally controlled by administration of doxycycline (DOX)-containing chow.

One of the *Met*^{ctg} functions as designed. When bred to CaMKII-tTA line (tTA+), the double mutants (ctg+:tTA+) can be identified by PCR (*, Fig. 1c). When ctg+:tTA+ mice were fed with regular chow without DOX (Fig. 1d), the tagged (FLAG) transgene product was readily detectable as a 140kd band in both PFC and HPC tissues at P22, which is devoid in the littermate control mice (ctg-;tTA-). In contrast, the band was not detected in the liver of ctg+:tTA+ mice, consistent with brain-specific expression. As a positive control, MET was also detected as a 170, 140kD double band in HEK293T cells transfected with the *Met* transgenic construct (pTRE-Tight-*cMet*-Myc-FLAG). Following detection of the FLAG tag, the blot was stripped and re-probed for total MET protein (both endogenous and transgenic). On average, there was a marked increase in MET protein (normalized to GAPDH) (Fig. 1d. $n = 3$, for both PFC and HPC). These data demonstrate that *Met* transgene is abundantly expressed in the absence of DOX and transcribed to produce a receptor protein.

We next ascertained whether *Met*^{ctg} can be controlled by DOX (Fig. 1e). The transgene was not detected at P7 in ctg+:tTA+ mice, likely due to the lack of CaMKII promotor activity at this age (25). By P16, transgene expression (Myc tag) was robust. Switching to DOX-chow for 5 d completely turned off the transgene when detected at P21. Removal of DOX thereafter for one week leads to re-expression of MET at P28. Transgene expression leads to dramatically increased MET phosphorylation (pY1234/1235) (> 5 fold increase) and increased total MET levels. The increased MET protein levels were additionally verified by increased immunostaining in the PFC and VC regions (Fig. 1f). Together, these data show that the approach used here to regulate transgene expression is effective in inducing controllable and sustained MET signaling beyond normal time windows of expression. In the following experiments, when crossed to the tTA line, these mice/dam were fed DOX-containing chow until P14, and then switched to DOX-free chow to turn on *Met* transgene expression. Unless otherwise stated, this strategy for controlled over-expression of MET is hereafter designated as *Met*^{coe}.

Sustained MET signaling alters synapse-enriched molecules in the developing visual cortex

Previous studies showed that *Met* cKO in the hippocampus results in altered biochemical composition of synaptic glutamate receptors, which correlated with an earlier maturation

profile of the CA1 synapse (13). We asked whether *Met*^{coe}, following endogenous MET signaling abatement, alters expression of synapse-enriched proteins. Using the strategy noted above, switching at P14 from DOX chow to regular chow enabled *Met*^{coe} in cortical excitatory neurons. Tissue punches were obtained from primary visual cortex (V1) and subjected to Western blot analyses of a panel of synapse-enriched proteins, glutamate receptors, and intracellular signaling proteins that are engaged by MET receptor activation and participate in the regulation of neuronal growth and signaling (27). We found a statistically significant reduction in GluA1, GluN2A, vGlut1, and Homer1 protein levels, whereas GluN2B was significantly increased (Fig. 2a). In comparison, other proteins, including inhibitory synapse marker vGAT and gephyrin, pan-neuronal marker neuN, presynaptic molecule synapsin I, excitatory synaptic protein CaMKIIα were not altered (Fig. 2b).

We also found an increased activation of small GTPases associated with *Met*^{coe}, as indicated by elevated levels of GTP-bound cdc42 and rac1, both of which are known to regulate neuronal growth and spine morphogenesis (28–30) (Fig. 2c). These biochemical experiments also identified that the downstream effectors of the small GTPase pathway are activated, as indicated by increased PAK1/2 activation through phosphorylation (T423/402), activation of LIMK1 (p-T508), and increased phosphorylation of cofilin (p-S3) (Fig. 2c). This analysis was replicated in 4–6 separate litters, with statistically confirmed changes (Fig. 2e–g). The decreased GluA1 and vGlut1 levels were further confirmed using IHC labeling and confocal imaging in the VC of P25 mice, noted as reduced IHC signal intensity (Fig. 2d, *n* =4). Together, these data demonstrate that eliminating the normal time-delimited down-regulation of MET by inducing expression of *Met*^{coe} results in less mature biochemical status of synapses, at a time when specific protein expression changes normally reflect more mature functional synapses.

Sustained MET signaling suppresses visual circuit maturation and function

To test the hypothesis that extending MET expression beyond the normal signaling period results in the maintenance of less mature excitatory synapses, functional measures of developing VC circuits were conducted. ctg+:tTA+ mice were fed with DOX chow until P14, and then switched to regular DOX free chow to induce *Met*^{coe} in cortical excitatory neurons (Fig. 3a). Littermate control mice (ctg-:tTA+ or ctg-:tTA-) underwent the same treatment. We first recorded miniature mEPSCs in layer (L) 5 pyramidal neurons with soma located in the anatomically defined binocular (bV1) region (16, 31) in P25 coronal tissue slices. Cumulative plots of mEPSC amplitude were constructed from > 4000 mEPSCs amplitude measurements for ctg+:tTA+ (*n* = 13 cells / 6 mice) and control groups (*n* = 11 cells, 6 mice) (Fig. 3b). K-S tests on the cumulative distribution showed a statistically significant reduction (p < 0.001) of mEPSC amplitude distribution in ctg+:tTA+ mice with approximately 2 weeks of MET over-expression. In addition, there was a statistically significant increase in mEPSC frequency. We next tested whether *Met*^{coe} affects inhibitory synaptic transmission by measuring mIPSCs in the same slice/animal. No significant differences were found in either mIPSC amplitudes (> 2500 events, 9 – 11 cells, 6 mice/ group) or mIPSC event frequency (Fig. 3b).

To determine whether there are changes in basic biophysical properties of L5 pyramidal neurons in *Met*^{coe} mice, a range of active and passive membrane properties were measured (Suppl. Fig. 2). There were no changes in membrane input resistance, soma capacitance, resting membrane potential (RMP), action potential (AP) threshold, rheobase current (minimum current injection that elicits AP), and current-action potential frequency relationships. These data indicate *Met*^{coe} does not affect VC L5 neuron membrane biophysical properties, including their intrinsic excitability.

We next conducted additional measurements related to synapse maturation and function. Whole cell responses from VC L5 pyramidal neurons were recorded in response to electric stimulation of L2/3 neurons (Fig. 3c). Only recordings exhibiting monosynaptic responses were included for analyses. Quantification of AMPA/NMDA receptor current ratio (A:N) for L5 pyramidal neurons from P25–28 mice revealed a dramatically reduced A:N ratio of *Met*^{coe} neurons (0.91 ± 0.09) compared to control neurons (1.34 ± 0.09) (Fig. 3c). Maturation of cortical circuits is reflected by increased GluN2B to GluN2A subunit switching (32, 33). We measured the pharmacologically isolated NMDA receptor current (in the presence of 20 μM CNQX) sensitivity to ifenprodil (3 μM) to estimate GluN2B subunit contribution to the NMDA current. The proportion of ifenprodil-induced reduction of charge transfer in *Met*^{coe} L5 neurons were significantly larger (48.4 ± 3.1%), compared with that from control L5 neurons (37.4 ± 3.1%) (Fig. 3d). These data indicate that *Met*^{coe} leads to relatively less AMPA receptor synaptic content and relatively more activation of NMDA receptors, particularly GluN2B-containing receptors.

Developmental VC maturation is also reflected by a reduction of silent synapses, which only contain NMDA receptors, but are capable of recruiting AMPA as a result of activity-dependent maturation (34). We quantified the proportion of silent synapses of the L2/3 to L5 circuit using a minimum stimulation protocol (Suppl. Fig. 3a–c) (35, 36). Neurons were first clamped at RMP (−65mV), and a minimum stimulus that elicited mixed responses and failures was adopted. Next neurons were voltage clamped at +40mV to collect additional successive trials (Suppl. Fig. 3a). Failure rates at −65mV were significantly greater in *Met*^{coe} neurons (50.3 ± 3.2%) than rates of control neurons (31.2 ± 3.1%) (Suppl. Fig. 3c). In addition, the percent difference of failure rates at these two potentials was significantly greater in *Met*^{coe} neurons (23.1 ± 2.0) compared to that from control neurons (13.4 ± 3.1) (Suppl. Fig. 3d). These data suggest that the normally sharp decrease in MET signaling by weaning in VC excitatory neurons is required for intralaminar synaptic maturation during the subsequent experience-dependent period of visual development.

Sustained MET signaling alters VC neuronal morphology

The altered spontaneous and evoked synaptic responses onto VC L5 pyramidal neurons suggest altered VC function. We asked whether *Met*^{coe} leads to structural alterations that would be consistent with altered maturation due to extended expression of MET. We filled L5 bV1 neurons with biocytin-containing internal recording solution and revealed neuronal morphology with avidin–Alexa 488 (Fig. 3e). Morphometric measures, including Sholl analysis (37), were obtained following neuron dendritic arbor reconstruction in three dimensions. In addition, Z stack confocal images were collected from apical dendrites of L5

pyramidal neurons in order to perform quantitation of spine morphometric parameters (see Methods). We found no significant change of neuronal dendritic arborization patterns in L5 neurons with Met^{coe} (Fig. 3f) ($p > 0.05$ for the group effect, two-way ANOVA). In contrast, analysis of the 3-D reconstructed dendritic spines from the apical dendrites of L5 neurons (Fig. 3g) revealed that Met^{coe} leads to increased dendritic spine density, increased spine length, and decreased spine head volume (Fig. 3h–j). The pooled spines (Fig. 3k, $n = 532$ spines/9 cells/5 mice) were classified into four main categories based on their geometry (38, 39). Further analysis revealed that compared with control neurons from littermates, Met^{coe} resulted in a significant decrease of the proportion of mature 'mushroom' type of spines ($\chi2 = 17.6$, p < 0.0001). This morphology change is indicative of immature morphology (40).

The observed alteration of mEPSC/mIPSC and spine phenotypes were not specific to VC L5 neurons, as L2/3 pyramidal neurons show a similar change in mEPSC amplitude and frequency, and a dendritic spine phenotype (Suppl. Fig. 4). These morphological findings on different VC excitatory neurons are consistent with the altered, immature spontaneous and synaptic responses associated with Met^{coe}, and lend further support to the hypothesis that normal down-regulation of MET is required for VC synapse development.

Disrupted visual cortex circuit connectivity by sustained MET expression

Next, we asked whether time-delimited signaling of MET is required for proper VC circuit connectivity. We used LSPS mapping (15, 19, 41) to probe synaptic connectivity made onto L2/3 pyramidal neurons in bV1 (17, 31). Met^{coe} and control mice were sacrificed at P25–32, during the VC critical period for binocular plasticity (18). L2/3 neurons were voltage clamped at −70mV (close to resting membrane potential), and UV laser pulses (1-ms, 20mW) were directed to a 16×16 location (with 75 μm spacing) spanning the entire VC cortical depth (Fig. 4a). Whole cell responses were acquired at each stimulus location, the amplitudes of which were used to construct a synaptic input map (Fig. 4b, c). After collecting LSPS maps from multiple neurons in each group, averaged maps revealed that L4 provides the strongest inputs to L2/3 pyramidal neurons in both groups (Fig. 4c). This is in agreement with the conserved laminar connectivity patterns in VC (42, 43). Further analysis of the averaged input maps show that Met^{coe} neurons receive statistically significantly altered synaptic inputs compared to control neurons (Fig. 4d, p < 001 for main genotype effect, two-way ANOVA). Strikingly, inputs from combined L4 locations were most significantly reduced (Fig. 4e). Surprisingly, the Met^{coe} L2/3 neurons receive significantly more inputs from non-L4 sources (Fig. 4f). These data indicate that sustained MET signaling in VC disrupts several features of intracortical connectivity, particularly input strength and connectivity topology.

Visual cortex critical period plasticity is impaired with sustained MET signaling

The changes in synapse maturation and intralaminar connectivity raised an important question regarding functional implications of atypical overexpression of MET. Plasticity and maturation of developing cortical circuitry are instructed by sensory experiences, which is extensively documented in the VC (44). Ocular dominance (OD) plasticity is a time-honored cortical plasticity paradigm, in which occluding vision to one eye during the critical period (P19–32 in the mouse (18, 45)) permanently degrades responsiveness to that eye in the VC.

In addition to altered inhibitory mechanisms (46–48), OD plasticity is known to involve local circuit reorganization and spine remodeling (49, 50). Based on the spine phenotypes, altered synaptic activity and connectivity, and our recent finding of disrupted timing of synaptic plasticity in hippocampus circuits in *Met* conditional knockout (cKO) mice (51), we hypothesized that VC circuit plasticity may be affected by disrupted timing of MET signaling. We adopted single unit recording in bV1 combined with a defined visual stimulus (Suppl. Fig. 5) to measure OD plasticity by calculating a contralateral bias index (CBI) (16, 20).

We first investigated the effects of *Met*^coe on MD-induced OD plasticity. In the continued presence of DOX-chow (no *Met*^coe), ctg+:tTA+ mice show normal OD plasticity when MD was initiated at P27–28 and lasted for 4–5 days, compared with non-deprived (ND) littermates of the same genotype [Fig. 5a, median (range) CBI scores, MD, 0.53 (0.49 – 0.58), *n* = 8 mice; ND, 0.64 (0.59–0.68), *n* = 8 mice. Mann-Whitney test]. In comparison, with removal of DOX at P14 to allow *Met*^coe, the MD protocol resulted in the elimination of OD plasticity during the normal critical period, illustrated by the lack of change in the CBI scores [Fig. 5b, median (range) of the CBI scores, MD, 0.64 (0.56–0.70), *n* = 9 mice; ND, 0.67 (0.61–0.71), *n* = 8 mice. p = 0.26].

Based on the temporal coincidence of endogenous MET down-regulation and the opening of the VC critical period (Fig. 1), and the absence of OD plasticity with sustained MET signaling, we next tested whether turning off *Met*^coe at a time that is well beyond the normal critical period (P40) would restore OD plasticity in bV1. ctg+:tTA+ mice were kept on DOX chow until P14, then switched to DOX-free chow to allow *Met*^coe. DOX-chow then was reintroduced on P40 to suppress ectopic MET expression. MD was conducted at P42–43 for 4–5 d, followed by OD plasticity testing/single unit recording at P47–8 (Fig. 5c). Non-visual deprived littermates of same genotype served as controls. As hypothesized, OD plasticity similar to that observed during the normal critical period (Fig. 5a) was evident at this late developmental stage [Fig. 5c, median (range) of the CBI scores, MD, 0.50 (0.39 – 0.61), *n* = 7 mice; ND, 0.65 (0.59 – 0.73), *n* = 8 mice]. To further validate that the reinstated OD plasticity is not a spurious effect of a dysregulated transgene approach, we conducted an additional experiment using ctg+:tTA+ mice that were kept on DOX-containing chow throughout the experiments (i.e., no *Met*^coe). As predicted, MD at P42–43 does not alter the CBI scores compared with the ND mice [Fig. 5d, median (range) of the CBI scores, MD, 0.65 (0.51 – 0.73), *n* = 8 mice; ND, 0.64 (0.55 – 0.72), *n* = 7 mice].

Based on these data indicating that sustained MET signaling impairs VC OD plasticity, which can be restored by terminating sustained MET expression even beyond the normal the critical period, we asked whether eliminating MET signaling may also impact the timing of OD plasticity. The *Met* conditional knockout (cKO) (*Met*^f/f;*emx1*^cre) prematurely eliminates MET signaling in developing excitatory cortical neurons (8, 13). Analyses of wild type (*Met*^f/f or Met^f/+, no cre) littermates reveals normal MD-induced OD plasticity during the critical period (P27–30) [Fig. 5e, CBI score: MD, 0.47 (0.38 – 0.57), *n* = 7 mice; ND, 0.66 (0.61–0.72), *n* = 9 mice. p = 0.002, Mann-Whitney U test]. Strikingly, in cKO mice, MD-induced OD plasticity was absent [Fig. 5e, CBI scores: MD, 0.62 (0.58 – 0.70); *n* = 7 mice; ND, 0.69 (0.61–0.71), *n* = 8 mice]. This suggests that in the absence

of MET signaling, critical period plasticity may not develop, or alternatively, closes earlier. We therefore performed experiments in cKO and littermate controls 5 d earlier, producing MD at P22–25. Control mice exhibited prominent OD plasticity [Fig. 5f, CBI score: MD, 0.52 (0.46 – 0.57), n = 8 mice; ND, 0.67 (0.64 – 0.72), n = 6 mice. p = 0.0007]. In cKO mice, statistically significant OD plasticity exists as well [Fig. 5f. CBI score: MD, 0.56 (0.49 – 0.62), n = 6 mice; ND, 0.65 (0.62 – 0.69), n = 7 mice. p = 0.002]. Thus, the cKO mice exhibit OD plasticity, but compared to WT mice, the critical period is abbreviated and ends prematurely. These data, combined with the findings from Met^{oe} mice, suggest that controlling the timing of MET signaling bi-directionally regulates the development of VC critical period plasticity.

DISCUSSION

The current study demonstrates that the temporally regulated expression of the MET receptor tyrosine kinase can regulate cortical circuit development and critical period plasticity in the primary visual cortex. These findings have implications for understanding the role of genetic variation that may not be causal for neurodevelopmental disorders (NDDs), but nonetheless may contribute significantly to disease phenotypes. Data presented here support the hypothesis that such regulation has pronounced effects on the maturation timing of developing neural circuits and experience-dependent circuit plasticity. *MET* is not a GWAS-significant gene causal for ASD, yet the combination of the 5' functional promoter allele (3) and other factors (52, 53) that cause dysregulation during synaptic maturation and plasticity may contribute to polygenic risk factors that influence the extent to which disorder-related phenotypes are manifested. We suggest that this may be one way of influencing the well-established clinical heterogeneity of NDDs, even in syndromic and rare single gene cases. The fact that *MET* gene and protein expression is reduced in two NDDs (ASD and Rett syndrome) (5, 6) raises the possibility that in those individuals with the largest expression changes, altered MET signaling contributes to brain circuit pathophysiology.

Using several experimental paradigms, we present evidence concerning key aspects of cortical circuit development that are broadly shaped by MET. We have previously shown that in MET-expressing developing hippocampal circuits, ablating MET signaling leads to profound changes of dendritic spine synapses, both structurally and functionally, and results in early maturation of the Schaffer collateral - CA1 synapse. In addition, we recently reported that in forebrain-specific *Met* cKO mice, the developing hippocampus CA1 synapses showed an enhanced long-term potentiation (LTP) and long-term depression (LTD) at early developmental stages (P12–14), whereas both LTP and LTD were reduced when mice reach young adulthood (P56–70) (51). These finding are consistent with the recent findings that *Met* cKO mice show altered responses to early life stress (54), and deficits in contextual fear learning (55). These studies, however, did not address directly the functional significance of *down-regulation* of MET and cessation of signaling. To gain insight into this issue, a controllable transgenic mouse line was created, utilizing a 'tet-off' strategy (56). Breeding this mouse line with CaMKII-tTA (25) mouse allows *Met* transgene expression and sustained signaling in cortical excitatory neurons that can be exquisitely controlled by DOX feeding. The data presented here demonstrate that sustained MET signaling in

excitatory neurons leads to extensive changes in the expression of key proteins involved in synaptic and circuit development, most notably altered expression of glutamate receptors and persistent activation of small GTPase pathways in the developing VC. Extending the duration of MET signaling also resulted in striking anatomical and functional changes of VC excitatory neurons in both L5 and L2/3, including smaller, immature, and supernumerary spines, which likely reflects a delay in synapse maturation. These structural and functional alterations are associated with disrupted topology of intralaminar VC connectivity, resolved here by LSPS circuit mapping.

We found that sustained or premature termination of MET signaling bi-directionally controls synaptic plasticity and the timing of the VC critical period, as measured by monocular deprivation-induced OD plasticity. The results demonstrate that *termination* of MET signaling is an essential component of critical period plasticity. Previous studies have shown that VC plasticity is associated with multiple mechanisms involving altered PV neuron-mediated inhibition (47, 57, 58), equilibrium of AMPA receptors (59), reorganization of intracortical connectivity (31), and dendritic spine pruning (49, 50). Given that MET is expressed in specific subtypes of L2/3 and 5/6 excitatory neurons (10), and not in cortical inhibitory neurons (60), data presented here show that sustained expression of MET is sufficient to eliminate developmental OD plasticity, suggesting a novel mechanism independent of local inhibitory influences (31). At a molecular level, we posit that this mechanism may involve altered dendritic spine structural plasticity, as continued MET signaling leads to sustained cofilin inhibition (Fig. 2). Another key discovery here was the ability to induce an ectopic period of heightened OD plasticity when the *Met* transgene was turned off at P40, a time when normal VC critical period is closed. Together with the observation of the dramatic down-regulation of MET protein just before the onset of the OD critical period in VC at 2–3 weeks age (18) (Fig. 1), these data suggest that termination of MET signaling is likely a conserved mechanism that facilitates opening of cortical critical period plasticity. Further supporting this hypothesis is the early closure of the critical period of OD plasticity when MET signaling was ablated in cortical excitatory neurons in the cKO mice. These findings are particularly significant considering the reports of altered sensory processing and critical period plasticity in Fragile X syndrome and Rett syndrome mouse models (61, 62).

There are several technical caveats regarding the reported studies. One issue in utilizing this transgenic approach is that expression levels of MET cannot be precisely controlled. Nonetheless, the extended duration of MET signaling is an important experimental manipulation to understand mechanistically the link between normal downregulation and neurodevelopmental outcomes. To our knowledge such overexpression strategy has not been reported for studying a gene whose expression is altered in neurodevelopmental disorders. Another issue is that although extended MET expression is driven in excitatory cortical neurons, our recent study (10) reported that only specific neuron subtypes dynamically express MET, particularly cortico-cortical neurons. While recognizing this weakness, concerns are mitigated due to the precise temporal control of *Met* transgene in the developing forebrain, the selective study of cellular and circuit phenotypes in excitatory neurons, the finding that *Met*^{ctg} engages relevant signaling pathways (e.g. pY1234/1235, small GTPases, p-cofilin) and reproduces similar cellular phenotypes as in single CA1

neuron manipulations (13), and the OD plasticity data resulting from the complementary studies that extended or eliminated *Met* transgene expression.

In summary, the results of these experiments provide new insights regarding mechanisms for controlling synapse maturation and plasticity at a circuit level in the developing neocortex. The role of MET receptor tyrosine kinase in cortical circuit development and the expression of critical period plasticity is linked to its time-delimited nature of signaling. These data suggest that MET during forebrain development may have broader implications for the development of synaptic plasticity, learning and memory, sensory perception, and adaptive behaviors, all of which may contribute to neuropathological changes in NDDs.

Supplementary Material

Refer to Web version on PubMed Central for supplementary material.

Acknowledgements

REFERENCE

1. Penzes P, Cahill ME, Jones KA, VanLeeuwen JE, Woolfrey KM (2011): Dendritic spine pathology in neuropsychiatric disorders. Nat Neurosci. 14:285–293. [PubMed: 21346746]

2. Zoghbi HY, Bear MF (2012): Synaptic dysfunction in neurodevelopmental disorders associated with autism and intellectual disabilities. Cold Spring Harb Perspect Biol. 4.

3. Campbell DB, Sutcliffe JS, Ebert PJ, Militerni R, Bravaccio C, Trillo S, et al. (2006): A genetic variant that disrupts MET transcription is associated with autism. Proc Natl Acad Sci U S A. 103:16834–16839. [PubMed: 17053076]

4. Aldinger KA, Lane CJ, Veenstra-VanderWeele J, Levitt P (2015): Patterns of Risk for Multiple Co-Occurring Medical Conditions Replicate Across Distinct Cohorts of Children with Autism Spectrum Disorder. Autism Res. 8:771–781. [PubMed: 26011086]

5. Campbell DB, D'Oronzio R, Garbett K, Ebert PJ, Mirnics K, Levitt P, et al. (2007): Disruption of cerebral cortex MET signaling in autism spectrum disorder. Ann Neurol. 62:243–250. [PubMed: 17696172]

6. Plummer JT, Evgrafov OV, Bergman MY, Friez M, Haiman CA, Levitt P, et al. (2013): Transcriptional regulation of the MET receptor tyrosine kinase gene by MeCP2 and sex-specific expression in autism and Rett syndrome. Transl Psychiatry. 3:e316. [PubMed: 24150225]

7. Rudie JD, Hernandez LM, Brown JA, Beck-Pancer D, Colich NL, Gorrindo P, et al. (2012): Autism-associated promoter variant in MET impacts functional and structural brain networks. Neuron. 75:904–915. [PubMed: 22958829]

8. Judson MC, Bergman MY, Campbell DB, Eagleson KL, Levitt P (2009): Dynamic gene and protein expression patterns of the autism-associated met receptor tyrosine kinase in the developing mouse forebrain. J Comp Neurol. 513:511–531. [PubMed: 19226509]

9. Lein ES, Hawrylycz MJ, Ao N, Ayres M, Bensinger A, Bernard A, et al. (2007): Genome-wide atlas of gene expression in the adult mouse brain. Nature. 445:168–176. [PubMed: 17151600]

10. Kast RJ, Wu HH, Levitt P (2019): Developmental Connectivity and Molecular Phenotypes of Unique Cortical Projection Neurons that Express a Synapse-Associated Receptor Tyrosine Kinase. Cereb Cortex. 29:189–201. [PubMed: 29190358]

11. Hensch TK (2005): Critical period plasticity in local cortical circuits. Nat Rev Neurosci. 6:877–888. [PubMed: 16261181]

12. Peng Y, Lu Z, Li G, Piechowicz M, Anderson MA, Uddin Y, et al. (2016): The autism associated MET receptor tyrosine kinase engages early neuronal growth mechanism and controls glutamatergic circuits development in the forebrain. Mol Psychiatry.

13. Qiu S, Lu Z, Levitt P (2014): MET receptor tyrosine kinase controls dendritic complexity, spine morphogenesis, and glutamatergic synapse maturation in the hippocampus. J Neurosci. 34:16166–16179. [PubMed: 25471559]

14. Gorski JA, Talley T, Qiu M, Puelles L, Rubenstein JL, Jones KR (2002): Cortical excitatory neurons and glia, but not GABAergic neurons, are produced in the Emx1-expressing lineage. J Neurosci. 22:6309–6314. [PubMed: 12151506]

15. Qiu S, Anderson CT, Levitt P, Shepherd GM (2011): Circuit-specific intracortical hyperconnectivity in mice with deletion of the autism-associated Met receptor tyrosine kinase. J Neurosci. 31:5855–5864. [PubMed: 21490227]

16. Stephany CE, Chan LL, Parivash SN, Dorton HM, Piechowicz M, Qiu S, et al. (2014): Plasticity of binocularity and visual acuity are differentially limited by nogo receptor. J Neurosci. 34:11631–11640. [PubMed: 25164659]

17. Stephany CE, Ikrar T, Nguyen C, Xu X, McGee AW (2016): Nogo Receptor 1 Confines a Disinhibitory Microcircuit to the Critical Period in Visual Cortex. J Neurosci. 36:11006–11012. [PubMed: 27798181]

18. Gordon JA, Stryker MP (1996): Experience-dependent plasticity of binocular responses in the primary visual cortex of the mouse. J Neurosci. 16:3274–3286. [PubMed: 8627365]

19. Suter BA, O'Connor T, Iyer V, Petreanu LT, Hooks BM, Kiritani T, et al. (2010): Ephus: multipurpose data acquisition software for neuroscience experiments. Front Neural Circuits. 4:100. [PubMed: 21960959]

20. Stephany CE, Ma X, Dorton HM, Wu J, Solomon AM, Frantz MG, et al. (2018): Distinct Circuits for Recovery of Eye Dominance and Acuity in Murine Amblyopia. Curr Biol. 28:1914–1923 e1915. [PubMed: 29887305]

21. Wiesel TN, Hubel DH (1963): Single-Cell Responses in Striate Cortex of Kittens Deprived of Vision in One Eye. J Neurophysiol. 26:1003–1017. [PubMed: 14084161]

22. Eagleson KL, Lane CJ, McFadyen-Ketchum L, Solak S, Wu HH, Levitt P (2016): Distinct intracellular signaling mediates C-MET regulation of dendritic growth and synaptogenesis. Dev Neurobiol. 76:1160–1181. [PubMed: 26818605]

23. Naldini L, Weidner KM, Vigna E, Gaudino G, Bardelli A, Ponzetto C, et al. (1991): Scatter factor and hepatocyte growth factor are indistinguishable ligands for the MET receptor. EMBO J. 10:2867–2878. [PubMed: 1655405]

24. Naldini L, Vigna E, Ferracini R, Longati P, Gandino L, Prat M, et al. (1991): The tyrosine kinase encoded by the MET proto-oncogene is activated by autophosphorylation. Mol Cell Biol. 11:1793–1803. [PubMed: 2005882]

25. Mayford M, Bach ME, Huang YY, Wang L, Hawkins RD, Kandel ER (1996): Control of memory formation through regulated expression of a CaMKII transgene. Science. 274:1678–1683. [PubMed: 8939850]

26. Robbins EM, Krupp AJ, Perez de Arce K, Ghosh AK, Fogel AI, Boucard A, et al. (2010): SynCAM 1 adhesion dynamically regulates synapse number and impacts plasticity and learning. Neuron. 68:894–906. [PubMed: 21145003]

27. Xie Z, Li J, Baker J, Eagleson KL, Coba MP, Levitt P (2016): Receptor Tyrosine Kinase MET Interactome and Neurodevelopmental Disorder Partners at the Developing Synapse. Biol Psychiatry.

28. Scott EK, Reuter JE, Luo L (2003): Small GTPase Cdc42 is required for multiple aspects of dendritic morphogenesis. J Neurosci. 23:3118–3123. [PubMed: 12716918]

29. Tashiro A, Minden A, Yuste R (2000): Regulation of dendritic spine morphology by the rho family of small GTPases: antagonistic roles of Rac and Rho. Cereb Cortex. 10:927–938. [PubMed: 11007543]

30. Yang N, Higuchi O, Ohashi K, Nagata K, Wada A, Kangawa K, et al. (1998): Cofilin phosphorylation by LIM-kinase 1 and its role in Rac-mediated actin reorganization. Nature. 393:809–812. [PubMed: 9655398]

31. Kuhlman SJ, Olivas ND, Tring E, Ikrar T, Xu X, Trachtenberg JT (2013): A disinhibitory microcircuit initiates critical-period plasticity in the visual cortex. Nature. 501:543–546. [PubMed: 23975100]

32. Monyer H, Burnashev N, Laurie DJ, Sakmann B, Seeburg PH (1994): Developmental and regional expression in the rat brain and functional properties of four NMDA receptors. Neuron. 12:529–540. [PubMed: 7512349]

33. Paoletti P, Bellone C, Zhou Q (2013): NMDA receptor subunit diversity: impact on receptor properties, synaptic plasticity and disease. Nat Rev Neurosci. 14:383–400. [PubMed: 23686171]

34. Lu W, Constantine-Paton M (2004): Eye opening rapidly induces synaptic potentiation and refinement. Neuron. 43:237–249. [PubMed: 15260959]

35. Liao D, Hessler NA, Malinow R (1995): Activation of postsynaptically silent synapses during pairing-induced LTP in CA1 region of hippocampal slice. Nature. 375:400–404. [PubMed: 7760933]

36. Qiu S, Weeber EJ (2007): Reelin signaling facilitates maturation of CA1 glutamatergic synapses. J Neurophysiol. 97:2312–2321. [PubMed: 17229826]

37. Sholl DA (1953): Dendritic organization in the neurons of the visual and motor cortices of the cat. J Anat. 87:387–406. [PubMed: 13117757]

38. Alvarez VA, Sabatini BL (2007): Anatomical and physiological plasticity of dendritic spines. Annu Rev Neurosci. 30:79–97. [PubMed: 17280523]

39. Ethell IM, Pasquale EB (2005): Molecular mechanisms of dendritic spine development and remodeling. Prog Neurobiol. 75:161–205. [PubMed: 15882774]

40. Matsuzaki M, Ellis-Davies GC, Nemoto T, Miyashita Y, Iino M, Kasai H (2001): Dendritic spine geometry is critical for AMPA receptor expression in hippocampal CA1 pyramidal neurons. Nat Neurosci. 4:1086–1092. [PubMed: 11687814]

41. Shepherd GM, Svoboda K (2005): Laminar and columnar organization of ascending excitatory projections to layer 2/3 pyramidal neurons in rat barrel cortex. J Neurosci. 25:5670–5679. [PubMed: 15958733]

42. Xu X, Callaway EM (2009): Laminar specificity of functional input to distinct types of inhibitory cortical neurons. J Neurosci. 29:70–85. [PubMed: 19129386]

43. Xu X, Olivas ND, Ikrar T, Peng T, Holmes TC, Nie Q, et al. (2016): Primary visual cortex shows laminar-specific and balanced circuit organization of excitatory and inhibitory synaptic connectivity. J Physiol. 594:1891–1910. [PubMed: 26844927]

44. Ko H, Cossell L, Baragli C, Antolik J, Clopath C, Hofer SB, et al. (2013): The emergence of functional microcircuits in visual cortex. Nature. 496:96–100. [PubMed: 23552948]

45. McGee AW, Yang Y, Fischer QS, Daw NW, Strittmatter SM (2005): Experience-driven plasticity of visual cortex limited by myelin and Nogo receptor. Science. 309:2222–2226. [PubMed: 16195464]

46. Gu Y, Huang S, Chang MC, Worley P, Kirkwood A, Quinlan EM (2013): Obligatory role for the immediate early gene NARP in critical period plasticity. Neuron. 79:335–346. [PubMed: 23889936]

47. Huang ZJ, Kirkwood A, Pizzorusso T, Porciatti V, Morales B, Bear MF, et al. (1999): BDNF regulates the maturation of inhibition and the critical period of plasticity in mouse visual cortex. Cell. 98:739–755. [PubMed: 10499792]

48. Pizzorusso T, Medini P, Berardi N, Chierzi S, Fawcett JW, Maffei L (2002): Reactivation of ocular dominance plasticity in the adult visual cortex. Science. 298:1248–1251. [PubMed: 12424383]

49. Majewska A, Sur M (2003): Motility of dendritic spines in visual cortex in vivo: changes during the critical period and effects of visual deprivation. Proc Natl Acad Sci U S A. 100:16024–16029. [PubMed: 14663137]

50. Zhou Y, Lai B, Gan WB (2017): Monocular deprivation induces dendritic spine elimination in the developing mouse visual cortex. Sci Rep. 7:4977. [PubMed: 28694464]

51. Ma X, Chen K, Lu Z, Piechowicz M, Liu Q, Wu J, et al. (2019): Disruption of MET Receptor Tyrosine Kinase, an Autism Risk Factor, Impairs Developmental Synaptic Plasticity in the Hippocampus. Dev Neurobiol. 79:36–50. [PubMed: 30304576]

52. Sheng L, Ding X, Ferguson M, McCallister M, Rhoades R, Maguire M, et al. (2010): Prenatal polycyclic aromatic hydrocarbon exposure leads to behavioral deficits and downregulation of receptor tyrosine kinase, MET. Toxicol Sci. 118:625–634. [PubMed: 20889680]

53. Volk HE, Kerin T, Lurmann F, Hertz-Picciotto I, McConnell R, Campbell DB (2014): Autism spectrum disorder: interaction of air pollution with the MET receptor tyrosine kinase gene. Epidemiology. 25:44–47. [PubMed: 24240654]

54. Heun-Johnson H, Levitt P (2018): Differential impact of Met receptor gene interaction with early-life stress on neuronal morphology and behavior in mice. Neurobiol Stress. 8:10–20. [PubMed: 29255778]

55. Thompson BL, Levitt P (2015): Complete or partial reduction of the Met receptor tyrosine kinase in distinct circuits differentially impacts mouse behavior. J Neurodev Disord. 7:35. [PubMed: 26523156]

56. Gossen M, Bujard H (1992): Tight control of gene expression in mammalian cells by tetracycline-responsive promoters. Proc Natl Acad Sci U S A. 89:5547–5551. [PubMed: 1319065]

57. Morishita H, Kundakovic M, Bicks L, Mitchell A, Akbarian S (2015): Interneuron epigenomes during the critical period of cortical plasticity: Implications for schizophrenia. Neurobiol Learn Mem. 124:104–110. [PubMed: 25849095]

58. Morishita H, Miwa JM, Heintz N, Hensch TK (2010): Lynx1, a cholinergic brake, limits plasticity in adult visual cortex. Science. 330:1238–1240. [PubMed: 21071629]

59. Han KS, Cooke SF, Xu W (2017): Experience-Dependent Equilibration of AMPAR-Mediated Synaptic Transmission during the Critical Period. Cell Rep. 18:892–904. [PubMed: 28122240]

60. Eagleson KL, Campbell DB, Thompson BL, Bergman MY, Levitt P (2011): The autism risk genes MET and PLAUR differentially impact cortical development. Autism Res. 4:68–83. [PubMed: 21328570]

61. Harlow EG, Till SM, Russell TA, Wijetunge LS, Kind P, Contractor A (2010): Critical period plasticity is disrupted in the barrel cortex of FMR1 knockout mice. Neuron. 65:385–398. [PubMed: 20159451]

62. Krishnan K, Wang BS, Lu J, Wang L, Maffei A, Cang J, et al. (2015): MeCP2 regulates the timing of critical period plasticity that shapes functional connectivity in primary visual cortex. Proc Natl Acad Sci U S A. 112:E4782–4791. [PubMed: 26261347]
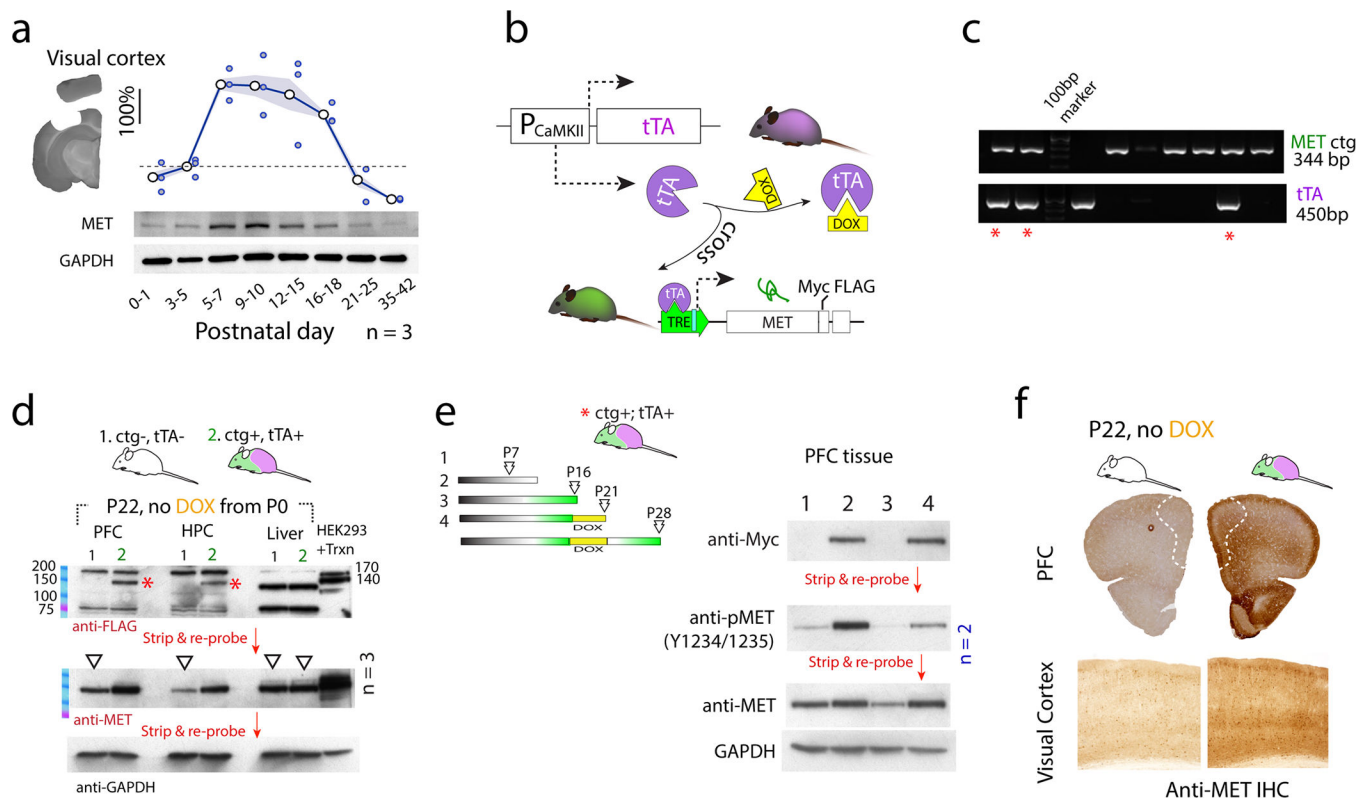
Fig. 1. Creation and validation of a controllable Met transgenic mouse line to achieve sustained MET expression and signaling.

a. MET protein expression was probed using Western blot across P0–42 in the visual cortex. GAPDH signal in the same blot was used to normalize MET signal. Quantification from three independent experiments were shown. Signal intensity was expressed as fold change compared to P3–5 levels. Shaded patches indicated s.e.m. **b.** Schematic illustration on the design of a controllable *Met* transgenic (*Met*^ctg) approach. **c.** Genotyping of double transgenic mice (*, ctg+;tTA+) by PCR.. **d.** When ctg+;tTA+ dam/litter were fed with DOX-free chow, transgene product (FLAG-tag) was detected at P22, no expression of *Met*^ctg was found in littermate controls (ctg-;tTA-). * 140-kD transgenic MET protein. No *Met*^ctg expression was found in the liver. Transfection of HEK293T cells with *Met*^ctg construct cDNA yields double bands (140, 170kD). The same blot was stripped and re-probed for MET, and GAPDH loading control proteins. **e.** Control of *Met*^ctg expression by DOX. No transgene was detected at P7. However, by P16 *Met*^ctg expression was abundant in the absence of DOX. Switching to DOX chow for 5 d completely turned off *Met*^ctg, after which adding back DOX-free chow for 7 d turned on *Met*^ctg. **f.** Increased MET IHC signal was observed in both PFC and VC with *Met*^ctg, indicating increased MET protein expression in these brain regions.
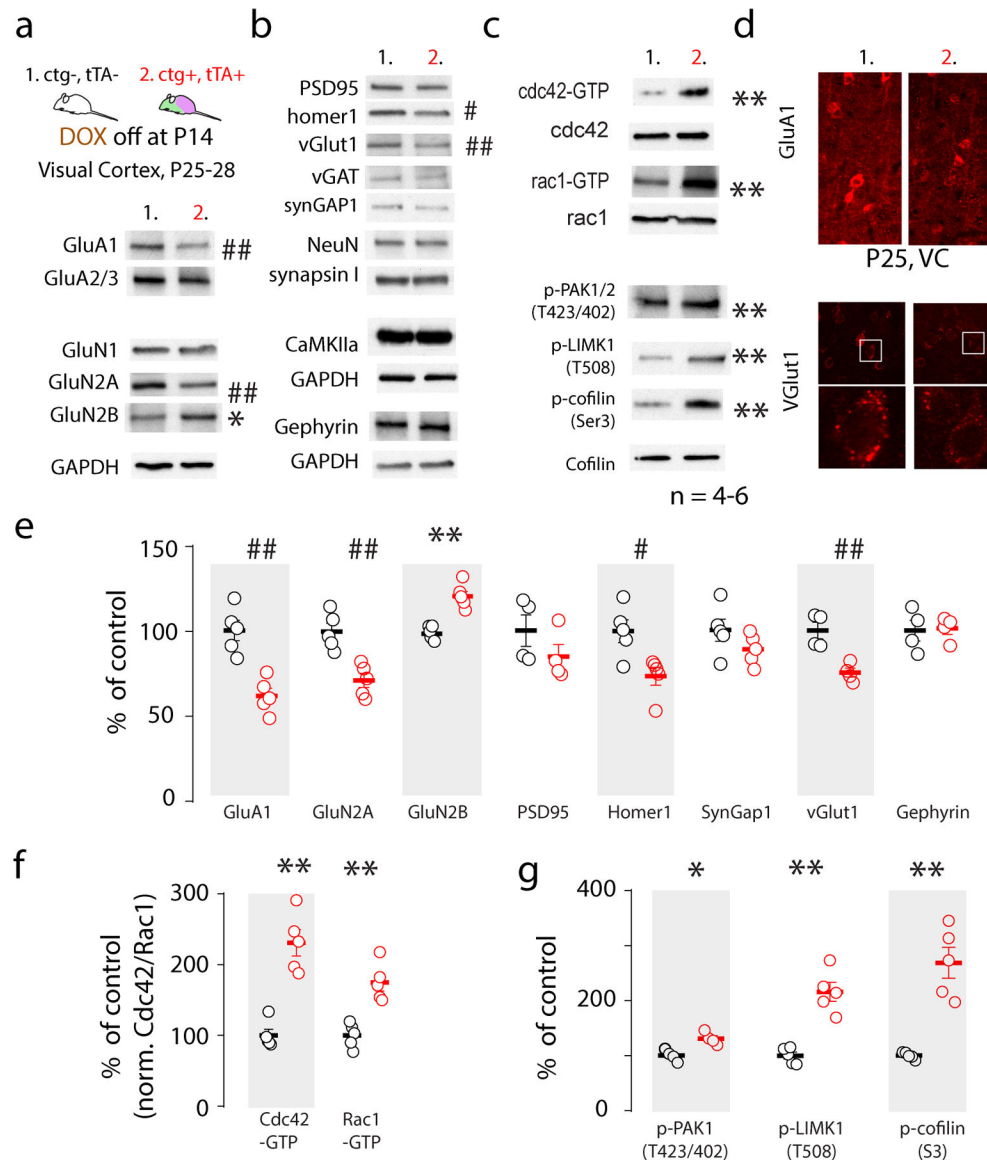
Fig. 2. Sustained expression of MET disrupts synapse proteins and neuronal growth mechanisms.

a. VC proteins were harvested at P25–28 in ctg+;tTA+ mice with sustained *Met*^{ctg} from P14 and control littermates. Representative blots showed decreased GluA1, GluN2A and increased GluB2B proteins. **b.** Among many synaptic proteins detected, sustained *Met*^{ctg} decreased Homer1 and vGlut1. **c.** *Met*^{ctg} leads to persistent activation of small GTPases cdc42 and rac1, and enhanced phosphorylation of PAK1/2 (T423/402), LIMK1 (T508), and cofilin (Ser 3). **d.** Decreased GluA1 and vGlut1 levels were verified using immunohistochemistry staining and confocal imaging. **e-g.** Quantification of Western blot (**a-d**) protein band intensity from 4–6 independent experiments. * p < 0.05, ** p < 0.01 (increase); # p < 0.05, ## p < 0.01 (decrease). cdc42-GTP, rac1-GTP and p-cofilin were normalized to cdc42, rac1 and cofilin, respectively, and expressed as percent of control levels.
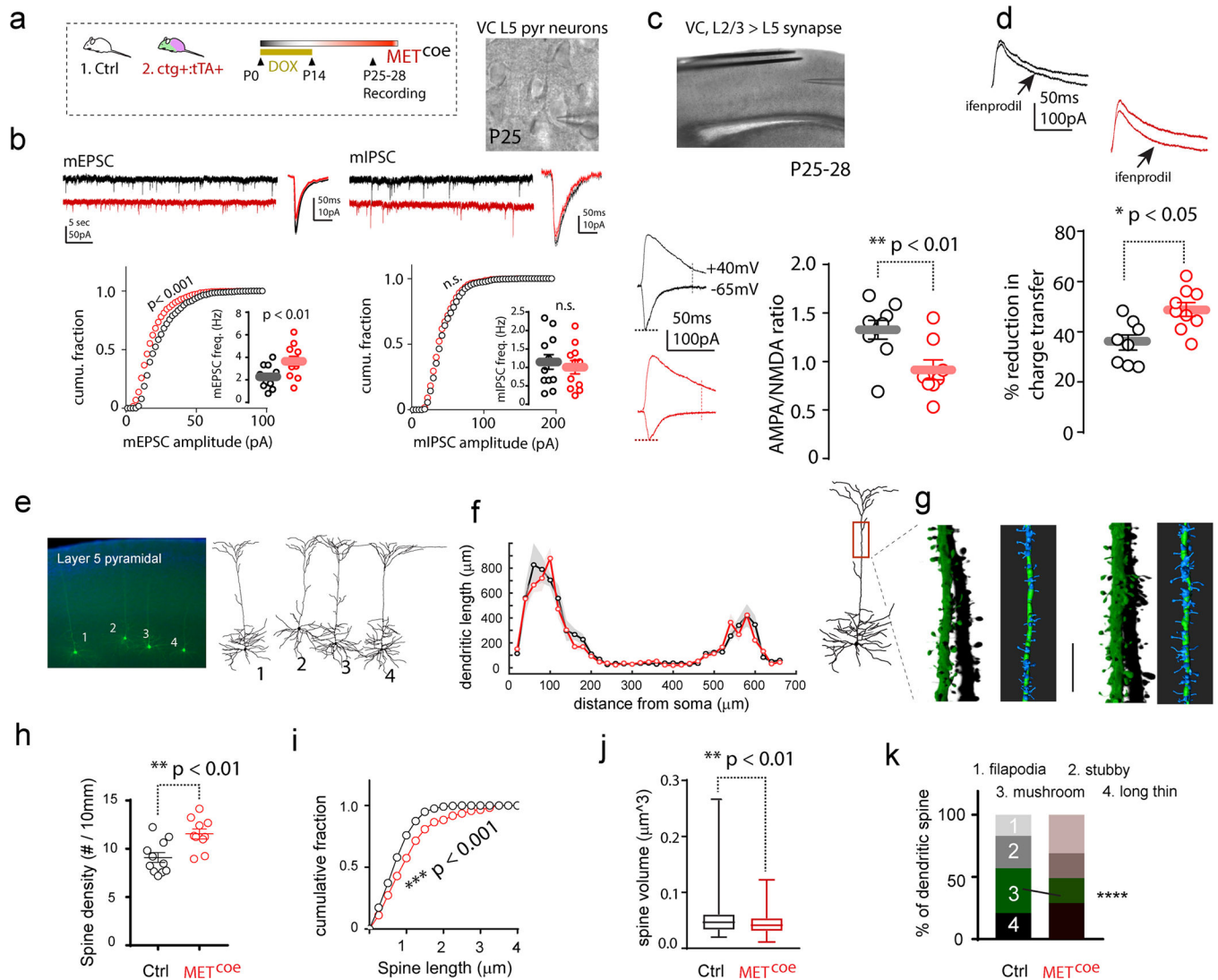
Fig. 3. Sustained MET expression disrupts VC L5 excitatory neuron structure and function.
a. Experimental design. Ctg+:tTA+ mice and littermate controls (Ctrl, ctg-:tTA+ or ctg-:tTA-) were kept on DOX chow until P14, followed by recording in VC brain slices at P25–28. **b.** *Met*coe L5 pyramidal neurons show decreased mEPSC amplitude (p < 0.001, K-S test), and increased mEPSC frequency (p < 0.01). In contrast, no change of mIPSC amplitude or frequency (n.s., p > 0.05 for both). **c.** Quantification of A:N ratio of synaptic responses in L5 neurons. A significant reduction of A:N ratio was found in *Met*coe (t_{15} = 3.05, ** p < 0.01). **d.** Ifenprodil sensitive current was also significantly increased in *Met*coe neurons (t_{15} = 2.45, * p < 0.05). **e.** Dendritic morphology of L5 neurons in anatomically defined bV1 were revealed by biocytin labeling. **f.** Sholl analysis of dendritic length distribution as a function of distance from soma. No significant difference was observed for genotype effects (p = 0.47, two-way ANOVA, n = 8 cells/5 mice, shaded patches, s.e.m.). **g.** Representative of three-dimension reconstruction of apical dendritic spines. **h-j.** *Met*coe leads to increased spine density (**h,** t_{19} = 3.37, ** p < 0.01), increased spine length (**i.** Ctrl, n = 179 spines/5 mice; METcoe, n = 150 spines/5 mice. K-S test, *** p < 0.001), reduced

spine head volume (**j.** Ctrl, n = 133 spines/4 mice; MET^{coe}, n = 186 spines/4 mice. **
p < 0.01. Man-Whitney U test). **k.** Percentage distribution of different categorical spine classifications. * p < 0.05, Chi-square test for the categorical spine counts and total spine numbers.
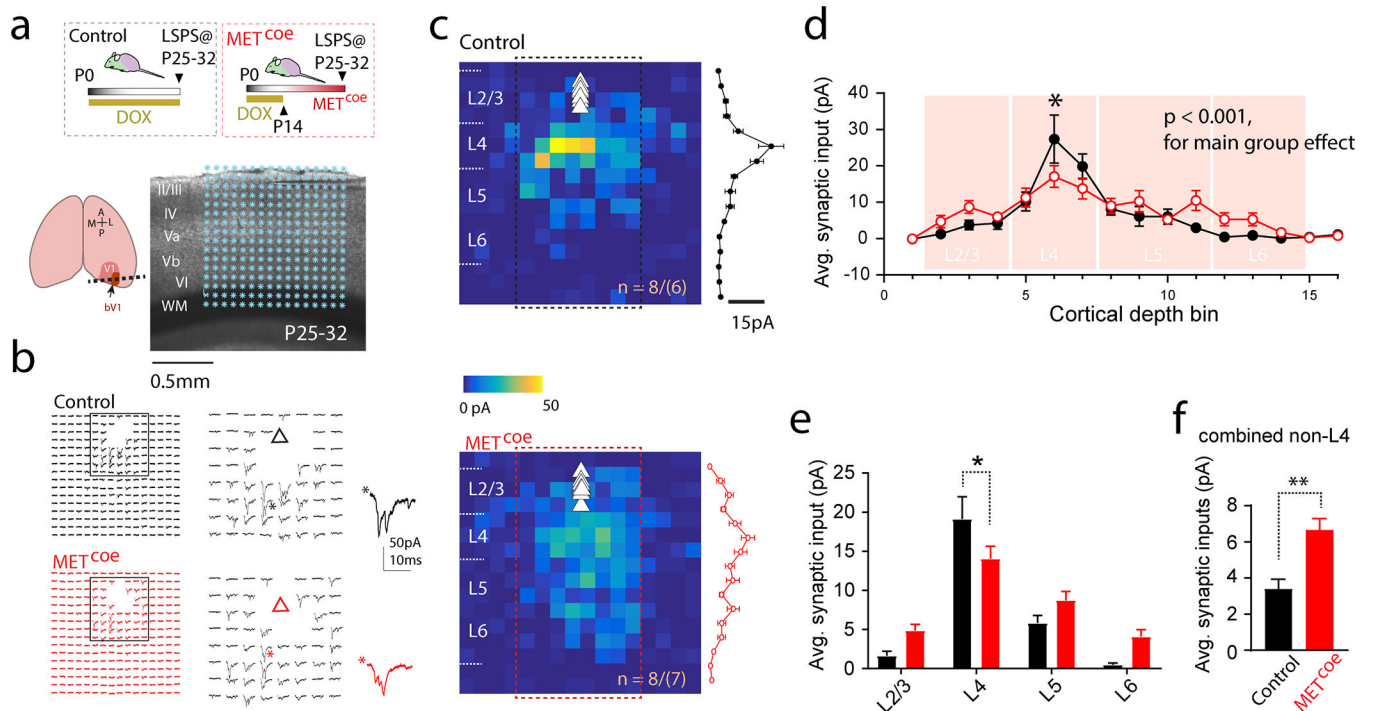
Fig. 4. Met^coe leads to altered intracortical connectivity in the bV1.
a. Illustration of VC slice preparation. A 16×16 LSPS mapping grid overlaid on DIC image (* denotes the glutamate uncaging locations), while L2/3 pyramidal neurons were voltage clamped at −70mV. **b.** Representative matrices of LSPS mapping traces from a control L5 pyramidal neuron, and a *Met*^coe L5 neuron. Triangle indicates soma position. **c.** Averaged color map from control (8 neurons/6 mice) and *Met*^coe (8 neurons/7 mice) mice. The EPSC amplitudes from center eight columns (boxed region) were averaged across the rows for each map, and pooled responses (mean ± s.e.m.) were plotted to the *right*. **d.** Synaptic inputs onto L2/3 neurons binned according to stimulus locations. Sidak's *post hoc* multiple comparison test revealed significantly reduced inputs from L4 (* p < 0.05). **e.** Averaged synaptic inputs from binned cortical layers. Significantly reduced L4 inputs were observed in *Met*^coe neurons (averaged L4 inputs: control, 19.1 ± 2.8 pA; *Met*^coe, 14.1 ± 1.6 pA. * p < 0.05, Sidak's multiple comparison test). **f.** L5 *Met*^coe neurons show significantly increased inputs from non-L4 sources (t_{14} = 3.94, p < 0.01. ** p< 0.01).
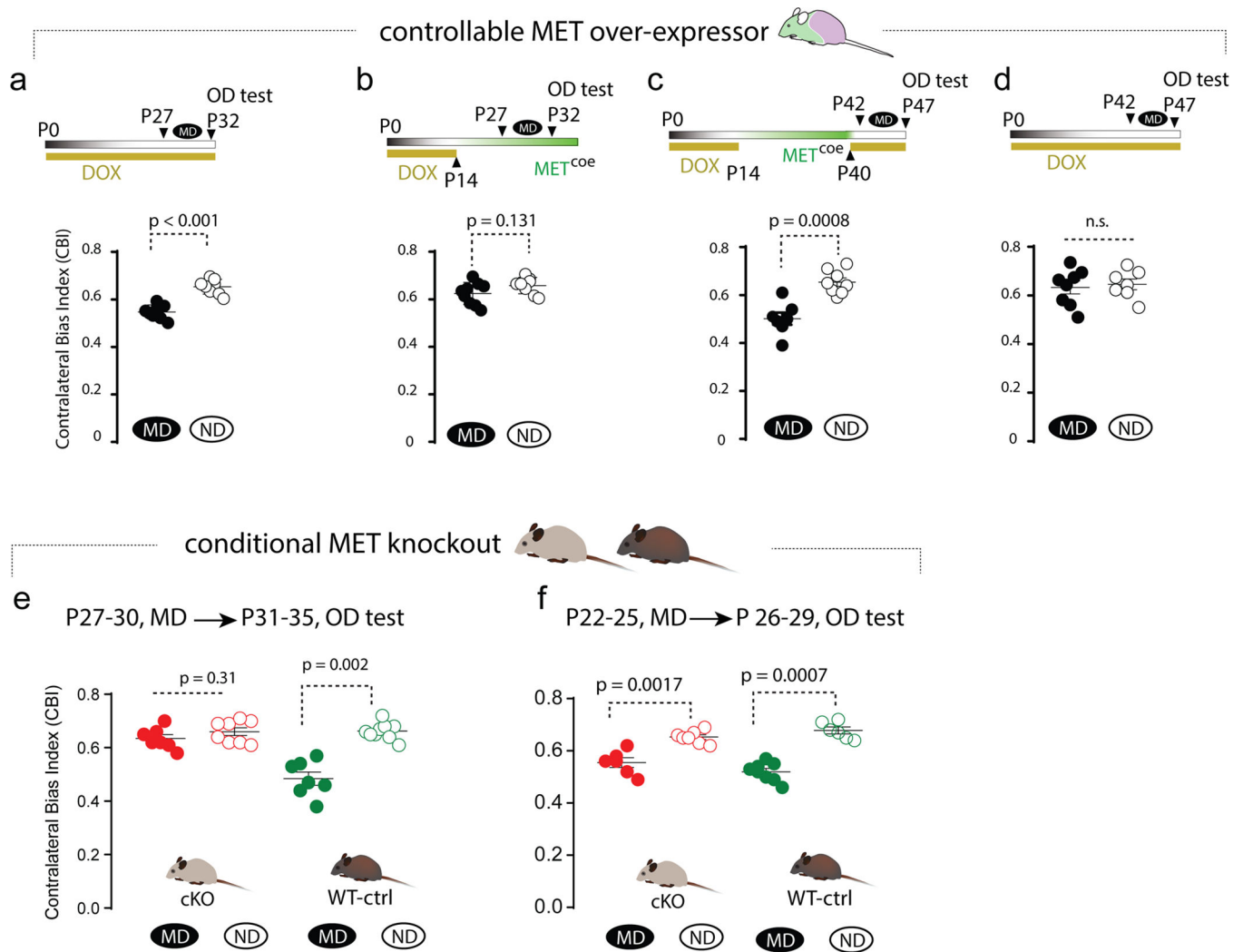
Fig. 5. Sustaining or eliminating MET signaling in developing forebrain alters the timing of VC critical period plasticity.
a. Normal MD-induced critical period plasticity was observed when *Met*^coe was suppressed by DOX, as MD induced significantly reduced CBI (p < 0.001). **b.** *Met*^coe from P14 eliminates critical period plasticity, measured at P32–33 as CBI by single unit recording. **c.** Extending MET signaling from P14-P40, followed by adding DOX to suppress MET signaling at P40, results in an ectopic period of heightened plasticity (p = 0.0008). **d.** Continued suppression of *Met*^ctg does not change the OD plasticity measured at P42, during which normal critical period is closed. **e.** Conditional *Met* knockout in forebrain excitatory neuron eliminates critical period plasticity when measured at P27-P30, during which control littermate exhibits normal plasticity. **f**. MD-induced OD plasticity in cKO mice exists at an earlier stage (P22–25). Each data point represents a mouse.